Determining the initial configuration and characterizing the mechanical properties of 3D angle-interlock fabrics using finite element simulation

Damien Durville, Ibrahim Baydoun, Hélène Moustacas, Guillaume Périé, Yanneck Wielhorski

Determining the initial configuration and characterizing the mechanical properties of 3D angle-interlock fabrics using finite element simulation

Damien Durville[a,*], Ibrahim Baydoun[a], Hélène Moustacas[a,b], Guillaume Périé[b], Yanneck Wielhorski[b]

[a] *MSSMat Laboratory, CentraleSupélec, CNRS UMR8579, Université Paris-Saclay*
[b] *Safran Aircraft Engines, Rond Point René Ravaud - Réau 77550 Moissy-Cramayel, France*

Abstract

A finite element simulation approach to the mechanical behaviour of 3D angle-interlock fabrics at the scale of their internal components, using an implicit scheme, is presented in this paper. Based on the determination of the static equilibrium of assemblies of fibres, this approach is used first to find the unknown initial configuration of a unit cell of angle-interlock fabric, by implementing an original method to gradually separate initially inter-penetrating yarns. This method, only based on the weaving pattern, does not require any geometrical pre-processor. Various loading cases can then be simulated to characterize the non-linear behaviour of such fabrics. Applications to the determination of the initial configuration of the unit cell of a typical example of a 5-layer angle-interlock fabric, and to the simulation of a transverse compression test and a forming test are presented.

Keywords:
3D angle-interlock fabric, finite element simulation, initial configuration, mechanical properties, transverse compression

*MSSMat Laboratory, CentraleSupélec, CNRS UMR8579, Université Paris-Saclay
Email address: damien.durville@centralesupelec.fr (Damien Durville)

1. Introduction

3D interlock fabrics are used as textile preforms for manufacturing composite parts with improved properties. Because the different layers of these fabrics are bound together by yarns passing through several layers, composites reinforced by 3D interlock fabrics offer improved resistance to delamination than conventional laminated composites. A better knowledge of both the internal micro-geometry and the mechanical behaviour of 3D interlock fabrics is required to optimize the mechanical properties of composites which incorporate them. The formability of the fabric, its ability to be impregnated by resin, as well as the local orientation of filaments within the composite part, are all dependant on the characteristics of the micro-geometry, in terms of trajectories and cross-sections of yarns, and fibre volume fraction within yarns.

Different approaches have been developed to characterize the micro-geometry of various kinds of 3D interlock fabrics. A review of these approaches, mostly aimed at determining the geometry of 3D woven composites in order to assess their mechanical properties using finite element analysis, can be found in [1]. Different works have led to the development of general geometrical pre-processors able to represent the geometry of different kinds of woven structures, among which WiseTex [2, 3, 4] and TexGen [5, 6, 7, 8, 9] are the best known. Some authors developed more refined analytical methods to get more accuracy in the determination of the internal geometry of 3D interlock fabrics[10, 11], or to take better account of contact surfaces between different tows [12]. Recent developments in X-ray computed tomography and related analysis tools provide an alternative way to recover the geometry of tows after segmentation of pictures obtained by tomography [13].

Besides these geometrical approaches, numerical simulation may also be employed to determine the micro-geometry of 3D interlock fabrics. First introduced to simulate the braiding process [14, 15], the digital element approach was extended in recent years to 3D interlock fabrics [16, 17, 18, 19, 20]. Starting from a first prediction of the micro-geometry based on the topology of the fabric, and discretizing each yarn into a set of digital fibres represented by rod elements connected by frictionless pins, this approach based on dynamic explicit solution scheme implements a relaxation procedure to determine the equilibrium of the fabric. Instead of using digital elements, tows constituting 3D interlock fabrics may also be represented by tubular structures allowing sufficient cross-sectional deformation, to determine ac-

curately the initial configuration of interlock fabrics, after a first prediction obtained with a geometrical pre-processor [21, 22].

This paper presents a finite element simulation approach, developed within a quasi-static framework and based on an implicit solution scheme, to determine the initial configuration of 3D angle-interlock fabrics, based mainly on the weaving pattern, without using any geometrical pre-processor. The proposed approach is implemented in an in-house simulation code, developed for the simulation of the mechanical behaviour of entangled fibrous materials, which determines the static equilibrium of assemblies of fibres or filaments, undergoing large displacements, and submitted to frictional contact interactions. Using a finite strain beam model, and focusing on the detection and modelling of frictional contact interactions [23], it allows the nonlinear behaviour of assemblies of fibres submitted to various loading cases to be identified. Previously applied to 2D woven fabrics [24, 25] and braided structures [26, 27], the present study extends the approach to the case of 3D angle-interlock fabrics. Compared to the weaving patterns employed for 2D fabrics, the pattern of the typical case of 3D interlock fabric considered in this study yields a more complex geometrical structure due to the intertwining between tows from the five different layers, and involves a higher number of tows to constitute the unit cell.

When the initial configuration of the considered structures can not be known a priori because it results from complex assembly processes, as in the case of woven [24, 25] or braided materials [26, 27], a procedure to determine this initial configuration has been developped. This procedure is adapted and applied to interlock fabrics in this paper. Starting from an arbitrary configuration, in which all yarns have straight trajectories and lie in the same plane, contact interactions determined by the simulation code are used to gradually separate interpenetrating yarns, in accordance with the weaving pattern. By this way the initial configuration, fulfilling the selected weaving pattern, is determined as a static equilibrium. Since yarns are represented by bundles of so-called macro-filaments, not only their trajectories, but also the shapes of their cross-sections can be captured. After the determination of the initial configuration, various loadings can be applied to the sample of interlock fabric so as to characterize its mechanical properties.

The paper is organized as follows. The next section presents the main bases of the adopted modeling to determine the static equilibrium of the assembly of filaments constituting a unit cell of 3D interlock fabric, including a macro-filament model, the detection and taking into account of frictional

contact interactions, and the consideration of hierarchical boundary conditions. Section 3 describes how the unknown initial configuration of the fabric is found by using contact interactions to gradually separate initially interpenetrating yarns. Application of the proposed methodology to a typical example of a 5-layer angle-interlock fabric is presented in the last section, covering the determination of its initial configuration, the simulation of a transverse compression test, and the simulation of the forming of the sample by means of analytical rigid surfaces.

2. Static equilibrium of a unit cell of 3D interlock fabric

The proposed modelling approach of interlock fabrics is developed within a quasi-static framework, and is aimed at determining the static equilibrium of a unit cell of fabric, considered as a hierarchically organized assembly of filaments, subject to frictional contact interactions. The mechanical problem is globally formulated in the same way for the stage of determination of the initial configuration and for the stage of simulation of different loading cases; the only differences between both stages lie in the way kinematical contact conditions between filaments are expressed. Because in most cases the number of filaments (typically few tens of thousands filaments per yarn) in the unit cell is much too high, a macro-filament model, representing bundles of filaments, is introduced and described below.

2.1. Principle of virtual work

The principle of virtual work characterizing the static equilibrium of the unit cell of fabric, constituted by N filaments or macro-filaments, is expressed as follows:

find $\boldsymbol{u}$ kinematically admissible, such that for each $\boldsymbol{v}$ kinematically admissible,

$$\sum_{I=1}^{N} W^I_{\text{beam}}(\boldsymbol{u},\boldsymbol{v}) + \sum_{I=1}^{N}\sum_{J=I+1}^{N} W^{IJ}_{\text{cf}}(\boldsymbol{u},\boldsymbol{v}) + \sum_{I=1}^{N} W^I_{\text{bc}}(\boldsymbol{u},\boldsymbol{v}) = 0, \tag{1}$$

where W^I_{beam} stands for the internal virtual work within filament (or macrofilament) I, W^{IJ}_{cf} for the virtual work of frictional contact interactions between filaments I and J, and W^I_{bc} for the virtual work resulting from the modelling of boundary conditions applied at ends of beam I. The way each of those three terms are computed is detailed hereafter.

2.2. Macro-filament model

The mechanical behaviour of elementary filaments or macro-filaments is represented using a finite strain beam model, in which the kinematics of any cross-section of the filament is described by means of three vectors: the position vector of the center of the cross-section, and two unconstrained directors [23]. This kinematics allows uniform and planar deformations of the cross-sections to be taken into account. The Green-Lagrange strain tensor derived from this model has no a priori zero term, and a standard 3D constitutive law can be used for the stress-strain relation. Using this model within a full Lagrangian framework, the internal virtual work for the filament (or macro-filament) I is expressed as:

$$W^I_{\text{beam}}(\boldsymbol{u}, \boldsymbol{v}) = \int_{\Omega^I_0} \text{Tr}\left(\boldsymbol{s}(\boldsymbol{u}) \frac{d\boldsymbol{E}(\boldsymbol{u})}{d\boldsymbol{u}} \cdot \boldsymbol{v}\right) d\omega, \tag{2}$$

where $\boldsymbol{E}$ stands for the Green-Lagrange strain tensor, $\boldsymbol{s}$ for the second Piola-Kirchhoff stress tensor, and Ω^I_0 for the initial configuration of filament I.

As is most cases, the number of filaments constituting a unit cell is far too high regarding simulation capabilities, a model of macro-filament is used to reproduce the behaviour of a bundle of filaments. A bundle of N_f filaments of radius r_f is assumed to be represented by an equivalent beam of radius r_M, called a macro-filament, whose axial stiffness is equal to the axial stiffness of the bundle, but whose flexural and torsional stiffnesses are significantly decreased to account for the mobility of filaments within the bundle under these loadings. In order to have the same cross-sectional area, the radius r_M of the macro-filament is determined as:

$$r_M = \sqrt{N_f} r_f, \tag{3}$$

and the same parameters are considered for the constitutive law. In order to adapt the flexural and the torsional stiffnesses of the macro-filament, in a first order approximation, individual filaments are assumed to deform independently from each other within the bundle under bending and twisting loadings. To reflect this, an adapted second moment of inertia, denoted I^*_M is considered for the macro-filament. This adapted moment of inertia is computed as:

$$I^*_M = N_f I_f, \tag{4}$$

where I_f is the second moment of inertia of individual filaments. With this adaption of the second moment of inertia of the macro-filaments, the values of

the flexural and torsional stiffnesses of the macro-filament correspond to those of the equivalent homogeneous beam, divided by the number of filaments constituting the macro-filament.

2.3. Frictional contact interactions

2.3.1. General approach for contact determination

Considering samples of fibrous materials, one is usually faced to a large number of varying contacts. The strategy employed to determine contacts in such media is briefly summarized here. Our approach is based on a multi-level search of contacts. At a first coarse level, proximity zones are determined between all pairs of possibly interacting filaments. So-called intermediate geometries, aimed at approximating the unknown actual contact zones are created for each proximity zone. These intermediate geometries then serve as geometrical supports for the discretization of contact-friction interactions. Discrete locations are regularly distributed along each intermediate geometry, and a contact element, constituted by a pair of material particles, is generated at each discrete location. This way of generating contact elements from intermediate geometries allows different contact configurations encountered in fabrics, ranging from contact between quasi-parallel filaments to contact between crossing filaments, to be considered.

2.3.2. Contact elements

A contact element $E_c(\zeta_k)$, generated at a given abscissa ζ_k of an intermediate geometry associated with a proximity zone between filaments I and J, is defined by the pair of material particles, located on the surface of both filaments, that are predicted to enter into contact at the position $\boldsymbol{x}_{int}(\zeta_k)$:

$$E_c(\zeta_k) = \left(\boldsymbol{\xi}^I(\zeta_k), \boldsymbol{\xi}^J(\zeta_k)\right) \in \Sigma^I \times \Sigma^J$$
$$\text{such that } \boldsymbol{\xi}^I(\zeta_k), \boldsymbol{\xi}^J(\zeta_k) \text{ are predicted to be likely to enter into contact in } \boldsymbol{x}_{int}(\zeta_k) \tag{5}$$

To determine the pair of material particles forming a contact element, cross-sections candidate to contact are first selected on both beams at intersections between a plane orthogonal to the intermediate geometry at $\boldsymbol{x}_{int}(\zeta_k)$, and the lines of centroids of both beams. The particles of the contact element are then located on the contours of these cross-section by geometric constructions.

2.3.3. Normal contact direction

A unit normal contact direction, denoted $\boldsymbol{N}(\zeta_k)$, is associated with each contact element. This direction is used to formulate a linearized kinematical

contact condition for this contact element, stating that the distance between the particles along this direction should remain positive, and expressed as:

$$g_N(E_c(\zeta_k)) = \left(\boldsymbol{x}^J\left(\boldsymbol{\xi}^J(\zeta_k)\right) - \boldsymbol{x}^I\left(\boldsymbol{\xi}^I(\zeta_k)\right), \boldsymbol{N}(\zeta_k)\right) \geq 0. \tag{6}$$

In standard situations, this normal contact direction is determined so as to prevent interpenetration between filaments. However, during the stage of determination of the initial configuration, which is characterized by large penetrations between filaments from different yarns, this normal direction is chosen so that interpenetrating filaments are repelled in the right directions, in accordance with the weaving pattern.

2.4. Hierarchical boundary conditions for a multi-level fibrous assembly

2.4.1. Introduction

A large numbers of degrees of freedom need to be controlled on the borders of the considered sample of interlock fabric. For the three level hierarchical organization of the fabric (into yarns, columns and layers) to be preserved, it is convenient to prescribe particular conditions to each of these levels. For this purpose, rigid bodies are attached to the ends of the components of different levels, namely yarns, columns and layers. In order to leave enough freedom to the displacements of components of different levels, averaged conditions are formulated on the borders of the sample to allow rearrangement.

2.4.2. Rigid bodies at ends of components of different levels

A rigid body is created and assigned to each end of the different components of the fabric. A rigid body is made of four rigidly connected nodes: one master node and three directional nodes defining the directions of a moving orthonormal coordinate system. To control its motions, both in translation and in rotation, different conditions can be prescribed to a rigid body, either in the global coordinate system or in a moving local coordinate system attached to a rigid body of upper level.

2.4.3. Formulation of averaged conditions

Considering a parent component and its sub-components (for example a column made of a set of yarns), the main advantage of the introduction of rigid bodies at ends of a component is to formulate boundary conditions at ends of its sub-components with respect to the moving coordinate system attached to the parent component. In order to let them the opportunity

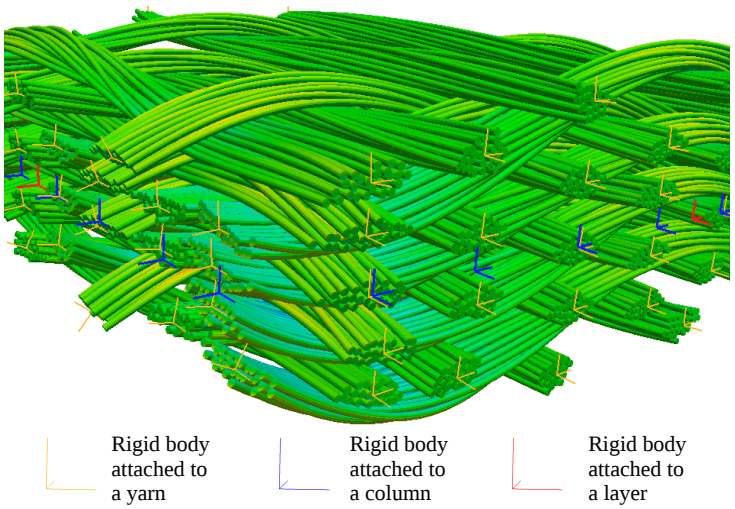

Figure 1: Rigid bodies attached to successive hierarchical levels within an interlock fabric

to rearrange, the conditions prescribed at ends of the sub-components of a given parent component can be formulated in average. For example, such a condition can be expressed in the following way:

$$\frac{1}{N_A}\sum_{a\in A}\left(\boldsymbol{x}_a - \boldsymbol{M}^A, \boldsymbol{D}_i^A\right) = 0, \tag{7}$$

where a is any of the N_A sub-components of the parent component A, where $\boldsymbol{x}_a$ stands for the position vector of the end of sub-component a, $\boldsymbol{M}^A$ for the position vector of the master node of the moving rigid body attached to the parent component and $\boldsymbol{D}_i^A$ for one of the directions defined by this rigid body. This condition states that, in the direction $\boldsymbol{D}_i^A$, the barycenter of ends of all sub-components of component A follows the position of the master node of the rigid body (Fig. 2).

In a similar way, it is also possible to control the average increment of rotation of all ends of a set of subcomponents about one axis $\boldsymbol{D}_i^A$ of the coordinate system associated with the rigid body of the parent component, by prescribing the following condition:

$$\frac{1}{N_A}\sum_{a\in A}\left(\Delta\boldsymbol{u}_a^n, \boldsymbol{d}_a^{\text{ortho}}\right) = 0, \tag{8}$$

where $\Delta\boldsymbol{u}_a^n$ is the increment of displacement at end of subcomponent a at step n, and $\boldsymbol{d}_a^{\text{ortho}}$ is the unit orthoradial direction at this end, defined with

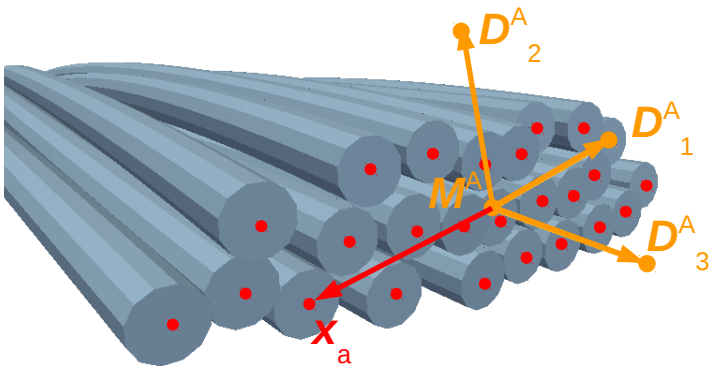

Figure 2: Coordinate system $\left(\boldsymbol{M}^A, \boldsymbol{D}_1^A, \boldsymbol{D}_2^A, \boldsymbol{D}_3^A\right)$ associated with the rigid body attached to one end of yarn

respect to the axis of rotation $\boldsymbol{D}_i^A$ associated with the rigid body of the parent component.

2.4.4. Periodic boundary conditions

In case the considered sample of fabric represents a periodic unit cell, periodic boundary conditions can be prescribed using the hierarchical conditions described above, by imposing that displacements at one end of a component are equal to those at the opposite end. At the level of macro-filaments, similar conditions can be prescribed to the directors of cross-sections at both ends in order to get same rotations. Periodic contact conditions on the borders of the sample are not yet accounted for.

3. Determination of the initial configuration by gradual separation of yarns

3.1. Introduction

The proposed approach to determine the unknown initial configuration of an interlock fabric presents itself as an alternative to the simulation of the actual weaving process. Simulating the weaving process at the scale of macro-filaments would involve much longer yarns, moved by complex motions, and would lead to huge computational cost. Instead of that, we start from an arbitrary configuration in which all yarns lie in the same plane, interpenetrating each other, and use contact interactions determined by the model, to gradually separate these yarns in accordance with the weaving pattern.

The main advantage of this method is the very small number of parameters required to determine the initial configuration. Since macro-filaments are assumed to be straight in the arbitrary starting configuration, the only parameters needed to define this configuration are the radii and lengths of macro-filaments, a description of their arrangement in each yarn according to a hexagonal pattern, and the distances between columns of yarns. The weaving pattern is simply described by an array of integers, taking their values in $\{-1, 0, 1\}$, which indicate the stacking order between any pair of yarns within the fabric. Denoting (T^i, T^j) a pair of yarns, the considered stacking order between these yarns, denoted $S\left(T^i, T^j\right)$, is defined as follows:

$$S\left(T^i, T^j\right) = \begin{cases} -1 & \text{if } T^i \text{ is in contact with } T^j \text{ and should remain below } T^j, \\ 1 & \text{if } T^i \text{ is in contact with } T^j \text{ and should remain above } T^j, \\ 0 & \text{otherwise.} \end{cases} \tag{9}$$

3.2. Adjusting the normal contact direction depending on the weaving pattern

When the approach is employed in standard situations where filaments are already separated from each other with only very small penetrations, the normal contact direction is computed from the positions of the centers of cross-sections so as to repel filaments and to resist to interpenetration. During the phase of determination of the initial configuration, during which macro-filaments are highly interpenetrating, the situation is different: the direction in which macro-filaments should be pushed back is no longer determined by the relative positions of macro-filaments, but by the stacking order related to the selected weaving pattern. For this purpose, during the phase of determination of the initial configuration, for a contact element generated between two macro-filaments M^I and M^J, belonging to two different yarns T^i and T^j, the adjusted normal contact direction $\boldsymbol{N}^*$ is determined in the following way:

$$\boldsymbol{N}^*(\zeta_k) = \begin{cases} -\boldsymbol{e}_z & \text{if } S\left(T^i, T^j\right) = -1, \\ \boldsymbol{e}_z & \text{if } S\left(T^i, T^j\right) = 1, \\ \boldsymbol{N}(\zeta_k) & \text{if } S\left(T^i, T^j\right) = 0, \end{cases} \tag{10}$$

where $\boldsymbol{e}_z$ denotes the vertical direction, and $\boldsymbol{N}$ the contact normal direction computed in the standard way.

3.3. Gradual reduction of interpenetrations

During the phase of determination of the initial configuration, before macro-filaments are separated, high interpenetrations or gaps (Eq. 6) are registered between filaments. In standard situations, the model used for contact interactions, based on a penalty method, should completely reduce the gap in one increment. When contact gaps are too high, reducing them in one step would yield too large increments of displacement for the non-linear algorithm to converge. During the determination of the initial configuration, to maintain increments of displacement sufficiently small to guarantee the convergence of non-linear algorithms, contact gaps are reduced gradually by definining a maximum gap reduction Δg_{red}. For each contact element, denoting g_{ini} the negative gap measured at the beginning of the increment, the adjusted normal contact gap, denoted g_N^* is determined as:

$$g_N^* = g_N - (g_{\text{ini}} + \Delta g_{\text{red}})\,. \tag{11}$$

Considering this modified gap g_N^* amounts to reduce the initial value at the beginnig of the step, g_{ini}, only by a value Δg_{red} (Fig. 3).

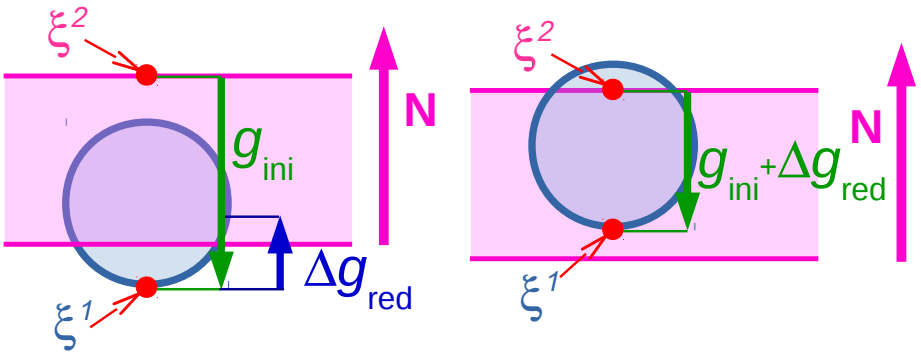

(a) Beginning of the increment (b) End of the increment

Figure 3: Gradual reduction of the gap during one increment

4. Determination of the initial configuration of a 3D angle-interlock fabric

4.1. Characteristics of the model

The proposed method to determine the initial geometry is applied to a typical example of a 5-layer angle-interlock fabric, made of carbon fibers. The

unit cell of the fabric is made of 36 weft yarns distributed into 8 columns, and 28 warp yarns distributed into 8 columns, totaling 64 yarns. Each yarn is represented by 25 macro-filaments. As real yarns are made of 48,000 carbon filaments, each macro-filament represents a bundle of 1920 real filaments with a radius of 2.5 μm. The total number of macro-filaments involved in the model is 1600. Main characteristics of the model are summarized in Table 1. The number of 25 macro-filaments to represent each yarn has been chosen to ensure a reasonable computational time for the determination of the initial configuration. Increasing the number of macro-filaments should improve the deformability of yarns' cross-sections. However, the different cross-section shapes observed either after the determination of the initial configuration (Figure 5), or at the end of the transverse loading test (Figure 10) appear satisfactorily deformed. Further comparisons with computed tomography images should be conducted to determine wether this number of macro-filaments is sufficient.

Number of weft yarns	36
Number of warp yarns	28
Total number of yarns	64
Number of macro-filaments per yarn	25
Total number of macro-filaments	1 600
Radius of macro-filaments	0.1095 mm
Young's modulus	276 000 MPa
Poisson's ratio	0.3

Table 1: Main characteristics of the model

4.2. Determination of the initial configuration

In the arbitrary starting configuration (Fig. 4), all yarns lie in the same plane, and the different yarns of each column are perfectly superimposed. A torsion is first applied at both ends of each yarn in order to consider an initial twist of about 200 turns per meter. The procedure of separation of yarns is then applied into 20 steps, by gradually reducing the large values of gaps corresponding to the initial inter-penetrations. Hierarchical boundary conditions are considered on the borders of the sample. Conditions in transverse directions for the different levels combine average conditions to allow rearrangement of the different components, and periodic conditions. A small tension is applied to each yarn to avoid buckling.

For each layer, in transverse directions (directions orthogonal to the yarns direction), a combination of averaged conditions and periodic conditions is considered so as to allow rearrangement of components of different levels (deformation of yarns cross-sections, misalignment of yarns in columns). In the longitudinal direction related to each layer, yarns are fixed at one end, while a small tensile force is applied at the opposite end. The consideration of the shrinkage of weft and warp yarns is made possible by the fact that yarns are only driven by tension at one end. Periodic conditions in the longitudinal direction are considered only at the level of macro-filaments, within each yarn.

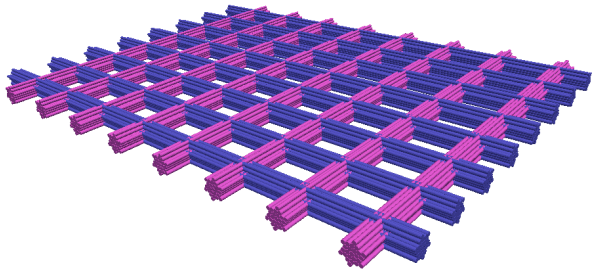

Figure 4: Arbitrary starting configuration for the 5-layer angle-interlock fabric unit cell

The evolution of the configuration during this procedure is shown in Figure 5. After the separation stage, standard contact conditions are considered, and the initial configuration which satisfies the static equilibrium is obtained (Fig. 6). The total CPU time needed for the determination of the initial configuration of this unit cell of fabric made of 1600 macro-filaments is about 30 hours, using four cores in parallel. Many interesting features, such as changes in yarn cross-sections, misalignments of yarns within columns, are captured by this simulation.

4.3. Reconstructing equivalent envelopes of yarns

In order to get a representation of the geometry of yarns, envelopes of the macro-filaments constituting each yarn can be reconstructed using the so-called "roughness roller" method introduced in [16], which consists in approximating the contour of a yarn cross-section by virtually rolling a cylinder of given radius on the surface defined by external macro-filaments. A major advantage of this method is that it allows non convex cross-sections to be

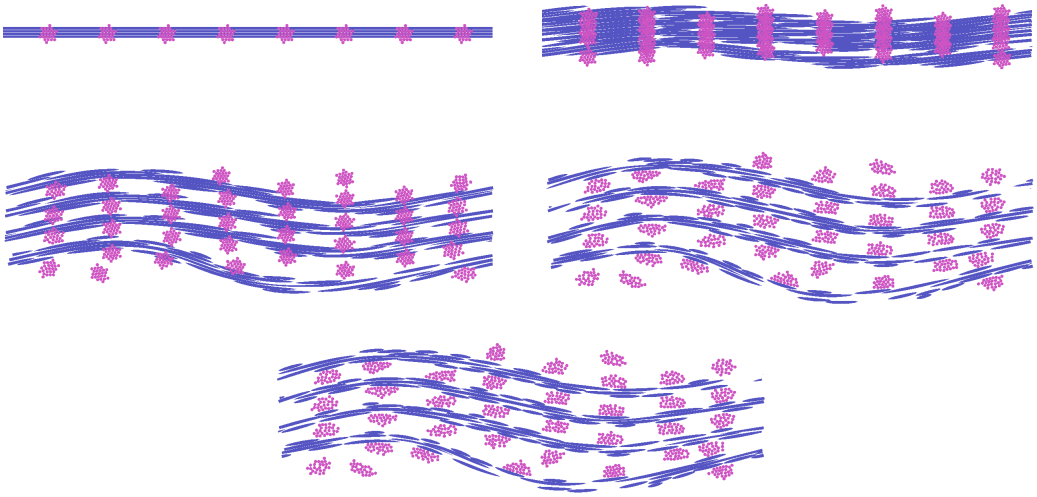

Figure 5: Cross-sections of the sample at intermediate steps during the process of determination of the initial configuration

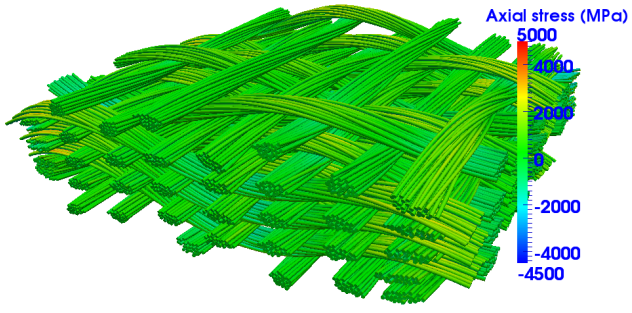

Figure 6: Determination of the initial configuration of a 5-layer angle-interlock fabric unit cell

determined. A roller with a radius equal to 15 times the radius of macro-filaments has been used to reconstruct the equivalent envelopes of yarns in the initial configuration, represented in Figures 7 and 8.

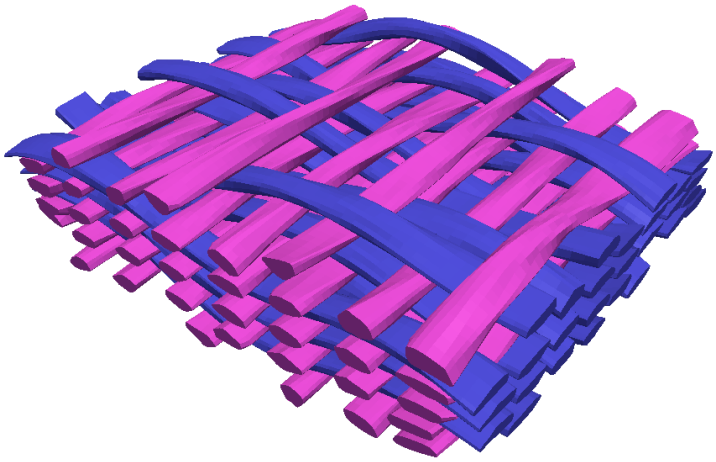

Figure 7: Equivalent envelopes of yarns in the initial configuration

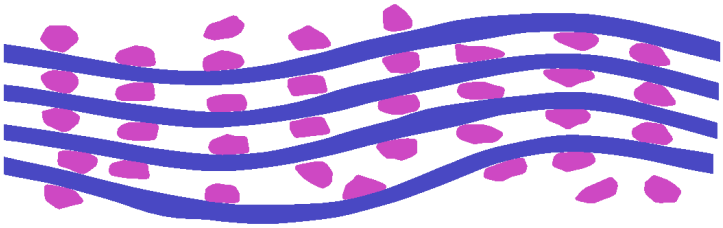

Figure 8: Cross-section of equivalent envelopes of yarns in the initial configuration

5. Simulation of loading tests

5.1. Transverse compression test

Once the initial configuration of the fabric has been determined, it can be used to simulate various loading tests aimed at characterizing the mechanical properties of the dry fabric. In order to simulate a transverse compression test, frictional contact interactions are considered between the macro-filaments of the fabric and two moving rigid planes. The distance between planes is gradually decreased, until dividing by two the initial thickness of

the dry fabric at rest (Fig. 9). This high transverse compression results in significant changes in both yarn trajectories and cross-sections, as it can be seen on the cross-sections of the studied sample (Fig. 10).

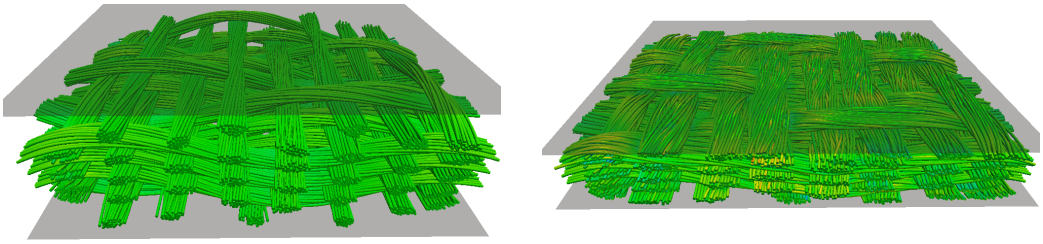

(a) Beginning of the transverse compression (b) End of the transverse compression

Figure 9: Simulation of a transverse compression test performed on the 5-layer angle-interlock fabric unit cell

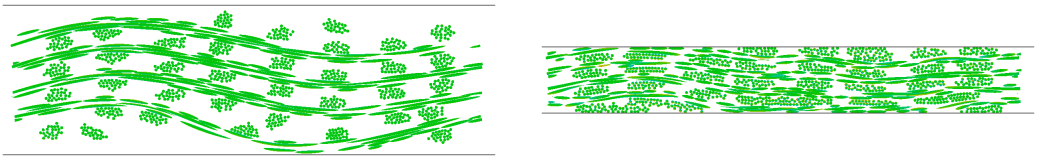

(a) Beginning of the transverse compression (b) End of the transverse compression

Figure 10: Simulation of a transverse compression test performed on the 5-layer angle-interlock fabric unit cell

The mechanical response of the dry fabric is highly nonlinear, with a strong increase of the transverse force as a maximum compaction is reached (Fig. 11).

5.2. Forming by rigid tools defined by analytical surfaces

As a last example, the forming of the sample of fabric by means of rigid tools made of a combination of planes and parts of cylinders is simulated (Fig. 12). The cylindrical shapes of the tools induce a combination of transversal and bending deformations within the fabric. This results in more complex motions at the scale of yarns and macro-filaments (Fig. 13). This example shows the ability of the model to describe local mechanisms taking place in such fabrics.

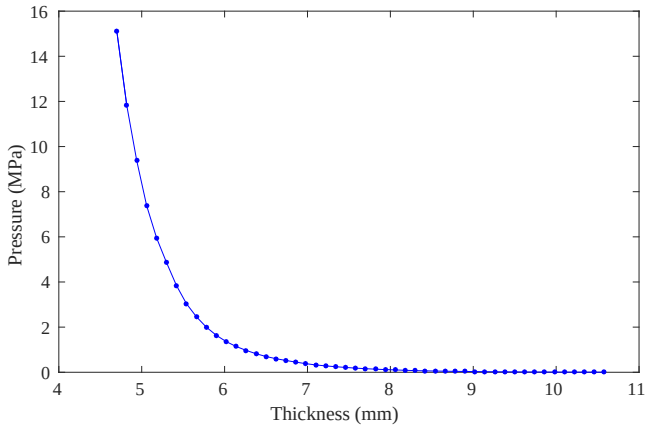

Figure 11: Loading curve (resulting pressure on moving planes) for the transverse compression test

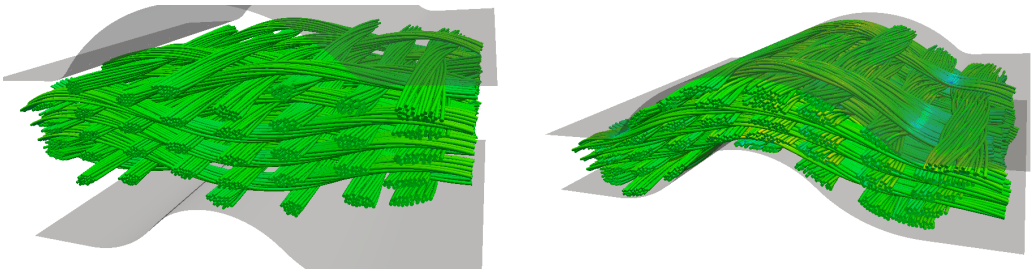

(a) Beginning of the loading

(b) End of the loading

Figure 12: Simulation of a forming test on the 5-layer angle-interlock fabric unit cell

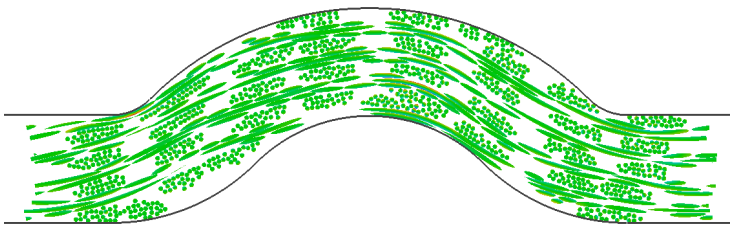

Figure 13: Cross-section of the 5-layer angle-interlock fabric unit cell at the end of the forming test

6. Conclusion

A finite element approach based on an implicit sheme, modelling frictional contact interactions within assemblies of fibres represented by finite strain beam elements, has been used in this paper for the determination of the unknown initial configuration of a typical example of a 3D angle-interlock fabric, and for the characterization of its mechanical properties under transverse loading, or during forming. Only few parameters are required to implement this approach based mainly on the weaving pattern, thus avoiding the use of a geometrical pre-processor. The detailed information provided by simulation results at the scales of yarns and macro-filaments should help better understand main mechanisms taking place within 3D angle-interlock fabrics in order to optimize mechanical properties of composite parts incorporating such reinforcements.

Acknowledgement

This work benefited from the support of the project INTERLOCK3D of the French National Research Agency (ANR).

References

[1] M. Ansar, W. Xinwei, Z. Chouwei, Modeling strategies of 3d woven composites: A review, Composite Structures 93 (8) (2011) 1947 – 1963.

[2] S. Lomov, A. Gusakov, G. Huysmans, A. Prodromou, I. Verpoest, Textile geometry preprocessor for meso-mechanical models of woven composites, Composites Science and Technology 60 (11) (2000) 2083 – 2095.

[3] I. Verpoest, S. V. Lomov, Virtual textile composites software wisetex: Integration with micro-mechanical, permeability and structural analysis, Composites Science and Technology 65 (15) (2005) 2563–2574.

[4] S. V. Lomov, Modelling the geometry of textile reinforcements for composites: Wisetex, in: P. Boisse (Ed.), Composite Reinforcements for Optimum Performance, Woodhead Publishing, 2011, pp. 200–238.

[5] M. Sherburn, Geometric and mechanical modelling of textiles, Ph.D. thesis, University of Nottingham (2007).

[6] A. Long, L. Brown, Modelling the geometry of textile reinforcements for composites: Texgen, in: P. Boisse (Ed.), Composite Reinforcements for Optimum Performance, Woodhead Publishing Series in Composites Science and Engineering, Woodhead Publishing, 2011, pp. 239 – 264.

[7] H. Lin, L. P. Brown, A. C. Long, Modelling and simulating textile structures using texgen, in: Advanced Materials Research, Vol. 331, Trans Tech Publ, 2011, pp. 44–47.

[8] H. Lin, X. Zeng, M. Sherburn, A. C. Long, M. J. Clifford, Automated geometric modelling of textile structures, Textile Research Journal 82 (16) (2012) 1689–1702.

[9] X. Zeng, L. P. Brown, A. Endruweit, M. Matveev, A. C. Long, Geometrical modelling of 3d woven reinforcements for polymer composites: Prediction of fabric permeability and composite mechanical properties, Composites Part A: Applied Science and Manufacturing 56 (2014) 150 – 160.

[10] N. Isart, B. E. Said, D. Ivanov, S. Hallett, J. Mayugo, N. Blanco, Internal geometric modelling of 3d woven composites: A comparison between different approaches, Composite Structures 132 (2015) 1219 – 1230.

[11] N. Isart, J. Mayugo, N. Blanco, L. Ripoll, A. Sol, M. Soler, Geometric model for 3d through-thickness orthogonal interlock composites, Composite Structures 119 (2015) 787 – 798.

[12] A. Wendling, G. Hivet, E. Vidal-Sall, P. Boisse, Consistent geometrical modelling of interlock fabrics, Finite Elements in Analysis and Design 90 (2014) 93 – 105.

[13] N. Naouar, E. Vidal-Salle, J. Schneider, E. Maire, P. Boisse, 3d composite reinforcement meso f.e. analyses based on x-ray computed tomography, Composite Structures 132 (2015) 1094 – 1104.

[14] Y. Wang, X. Sun, Digital-element simulation of textile processes, Composites Science and Technology 61 (2) (2001) 311 – 319.

[15] G. Zhou, X. Sun, Y. Wang, Multi-chain digital element analysis in textile mechanics, Composites Science and Technology 64 (2) (2004) 239 – 244.

[16] L. Huang, Y. Wang, Y. Miao, D. Swenson, Y. Ma, C.-F. Yen, Dynamic relaxation approach with periodic boundary conditions in determining the 3-d woven textile micro-geometry, Composite Structures 106 (2013) 417 – 425.

[17] Y. Mahadik, S. Hallett, Finite element modelling of tow geometry in 3d woven fabrics, Composites Part A: Applied Science and Manufacturing 41 (9) (2010) 1192–1200.

[18] S. Green, A. Long, B. E. Said, S. Hallett, Numerical modelling of 3d woven preform deformations, Composite Structures 108 (2014) 747 – 756.

[19] L. Daelemans, J. Faes, S. Allaoui, G. Hivet, M. Dierick, L. V. Hoorebeke, W. V. Paepegem, Finite element simulation of the woven geometry and mechanical behaviour of a 3d woven dry fabric under tensile and shear loading using the digital element method, Composites Science and Technology 137 (2016) 177 – 187.

[20] S. Joglekar, M. Pankow, Modeling of 3d woven composites using the digital element approach for accurate prediction of kinking under compressive loads, Composite Structures 160 (2017) 547 – 559.

[21] F. Stig, S. Hallström, Spatial modelling of 3d-woven textiles, Composite Structures 94 (5) (2012) 1495 – 1502.

[22] F. Stig, S. Hallström, A modelling framework for composites containing 3d reinforcement, Composite Structures 94 (9) (2012) 2895 – 2901.

[23] D. Durville, Contact-friction modeling within elastic beam assemblies: an application to knot tightening, Computational Mechanics 49 (2012) 687–707.

[24] D. Durville, Simulation of the mechanical behaviour of woven fabrics at the scale of fibers, International journal of material forming 3 (2) (2010) 1241–1251.

[25] D. Durville, Microscopic approaches for composite reinforcement mechanical behaviour, in: P. Boisse (Ed.), Composite reinforcements for optimum performance, Woodhead Publishing, 2011, pp. 461–485.

[26] T. Vu, D. Durville, P. Davies, Finite element simulation of the mechanical behavior of synthetic braided ropes and validation on a tensile test, International Journal of Solids and Structures 58 (2015) 106 – 116.

[27] P. Davies, D. Durville, T. D. Vu, The influence of torsion on braided rope performance, modelling and tests, Applied Ocean Research 59 (2016) 417 – 423.